CHEMISTRY OF MATERIALS
Article

Chem. Mater. **2010,** *22,* 4591–4601 4591
DOI:10.1021/cm100672u

Enantioselective Adsorption Characteristics of Aluminum-Substituted MFI Zeolites

Tom P. Caremans,[†] Titus S. van Erp,*[,†] David Dubbeldam,[‡] Juan Manuel Castillo,[#] Johan A. Martens,[†] and Sofia Calero[¶]

[†]*Centrum voor Oppervlaktechemie en Katalyse, K.U. Leuven, Kasteelpark Arenberg 23, B-3001 Leuven, Belgium,* [‡]*Van't Hoff Institute for Molecular Sciences, University of Amsterdam, Nieuwe Achtergracht 166, 1018 WV Amsterdam, The Netherlands,* [#]*Process & Energy Laboratory, Delft University of Technology, Delft, The Netherlands, and* [¶]*Department of Physical, Chemical, and Natural Systems, University Pablo de Olavide, Ctra. Utrera km 1, 41013 Seville, Spain*

Received March 5, 2010. Revised Manuscript Received June 25, 2010

Using computer simulations, we have studied the adsorption of racemic and scalemic mixtures of 4-ethyl-4-methyloctane molecules in aluminum-substituted MFI zeolites containing positively charged ions. Our results show that aluminum distribution affects the shape of the enantiopure adsorption isotherms, which is contrary to previously established results on linear alkanes. In addition, we examined the enantiospecific adsorption at maximum loading conditions. For enantiopure and racemic mixtures, the fraction of S- and R-enantiomers in the adsorbed phase is identical to that of the gas phase. However, when the external gas contains a scalemic mixture, the dominant enantiomeric fraction might either increase or decrease upon adsorption, depending on the aluminum distribution and on the type of cations. We provide a theoretical explanation for both types of adsorption characteristics. Our findings open perspectives for new approaches of enantioseparation that do not require a chiral adsorbent.

Introduction

The large majority of drug molecules are chiral. In 2006, 80% of the small-molecule drugs approved by the U.S. Food and Drug Administration (FDA) were chiral, and 75% were single enantiomers.[1] For many chiral drugs, only one of the enantiomers will have the desired therapeutic effects, whereas the other component might be poisonous. Nowadays, a new medicine can be sold under its racemic form, but a full characterization of the pharmacological and toxicological effects of the single enantiomers, as well as their combination, is required. Therefore, reliable enantioselective separation processes are essential unit operations of pharmaceutical production.[2] Industrial separation of enantiomers is, in most cases, achieved by chiral column chromatography. This technique exploits small differences in adsorption and migration of the two types when guided through a suitable chiral solid material.[3] Chiral adsorbents can be synthesized, for instance, by grafting molecular chiral modifiers on a stationary phase.[4] However, the process is expensive and only applicable to a limited number of chiral molecules.

An interesting possibility is the use of zeolites. Zeolites, which are composed essentially of silicon and oxide, are relatively inexpensive and have excellent durability. The high silica content makes it resistant to the high temperatures that are encountered during catalytic and regeneration cycles. The interest in zeolites in technological areas is explained by their appealing physicochemical properties. Zeolites are characterized by a high specific surface area and microporosity. The effective pore sizes in zeolites range from 0.4 nm to >1.3 nm,[5] which permits the diffusion of catalytically interesting molecules. The critical parameters are the shape of the pores and the free apertures of the windows giving access to the cages. This is the main reason for the everlasting intensive search for new zeolite topologies. Nowadays, zeolites play an important role in various fields of technology, ranging from catalysts in petroleum refining, petrochemistry intermediates and fine chemistry, renewable chemicals and fuels, pollution abatement via exhaust gas and wastewater treatment, and cation exchange.[6] Zeolites are also used to separate mixtures of hydrocarbons, because their large specific surface area and pore sizes of molecular dimensions provide them with unique sieving properties.[7]

A long-standing question in the zeolite technology area is whether sterical restrictions could be exploited to realize chiral separation. The development of robust zeolite materials for chiral separation would present a major technological breakthrough. In achieving this, much research has been focused on the synthesis of chiral zeolite topologies. So far, the development of zeolite adsorbents for separation of chiral

*To whom correspondence should be addressed. E-mail: Titus.VanErp@biw.KULeuven.be.

(1) Thayer, A. M. *Chem. Eng. News* **2007**, *85*, 11–19.
(2) Gubitz, G.; Schmid, M. G. *Mol. Biotechnol.* **2006**, *32*, 159–179.
(3) Allenmark, S. *Chromatographic Enantioseparation: Methods and Applications*; Ellis Horwood: Chichester, England, 1991.
(4) Maier, N. M.; Franco, P.; Lindner, W. *J. Chromatogr. A* **2001**, *906*, 3–33.
(5) Davis, M. E.; Lobo, R. F. *Chem. Mater.* **1992**, *4*, 756–768.
(6) *Zeolites for Cleaner Technologies*; Guisnet, M., Gilson, J.-P., Eds.; Imperial College Press: London, 2002; Vol. *3*.
(7) Denayer, J. F. M.; De Meyer, K.; Martens, J. A.; Baron, G. V. *Angew. Chem.−Int. Ed.* **2003**, *42*, 2774–2777.

Published on Web 07/29/2010

molecules has faced limited success. Theoretically, numerous chiral zeolite topologies are possible, but the vast majority of synthesized zeolites have achiral structures. Only $<3\%$ of the zeolites known to date are chiral,[8−12] and most of these structures are thermally unstable. The structure collapses upon calcination and evacuation of the pores, preventing their application. Moreover, the asymmetry in the structure is usually developed on a length scale of several nanometers and, therefore, is less appropriate for recognition by the smaller molecules. Attempts to synthesize zeolites using chiral templates turned out to be achiral.[13] Alternative approaches try to incorporate chiral modifiers in zeolite pores[14,15] or to block selectively one type of pores in a heterochiral zeolite. Molecular simulation techniques have evaluated this last possibility for Polymorph A of zeolite β, which has pores of opposed chirality.[16]

Recently, we demonstrated a fundamentally new approach to utilize zeolites for enantioseparation.[17] If the gas consists of a scalemic mixture, in which one enantiomer is already present in higher concentrations than the other, the initial molecules that adsorb can create an effective chiral environment for the next ones. Although the principle is very general, it requires a very specific match between the chiral molecules and the zeolite topology. A proof-of-concept was demonstrated for small chiral hydrocarbons in aluminum-substituted MFI zeolites in the presence of cations.[17] Here, we present a detailed analysis of this enantiospecific adsorption effect. Our theoretical model, based on the concept of chiral cells,[17] is able to explain and predict both heteroselective and homoselective adsorption. This model might be a very useful tool for future technological developments that try to exploit this enantiospecific adsorption effect. This phenomenon might ultimately be used to establish entioseparation of commercially or pharmaceutically relevant molecules.

Methodology

Models. 4-ethyl-4-methyloctane is the simplest chiral saturated hydrocarbon with a quaternary stereogenic center. It comprises a central carbon with a methyl, ethyl, propyl, and butyl group tetrahedrally attached to it, such that that it either forms the left- or right-handed form (S- or R-enantiomer; see Figure 1). The wealth of information on adsorption equilibria, and the availability of accurate force fields for hydrocarbons in zeolites,[18] makes

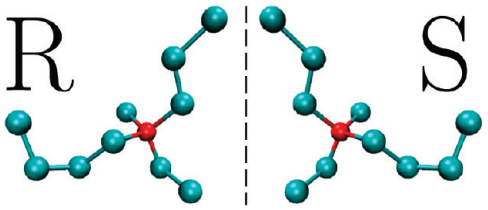

Figure 1. R- and S-enantiomeric form of 4-ethyl-4-methyloctane.

it an ideal candidate for our study. 3-Methylhexane is an even simpler chiral hydrocarbon, but it has a computational drawback. The central carbon is connected to a propyl group, an ethyl group, and a methyl group and is further connected to a single hydrogen that is normally not explicitly described by the united atom model. As result, there is no steric repulsion from this side, which eventually allows the C_1, C_2, and C_3 branches to surpass planar configuration and bend further to the other side, where it changes its enantiomeric identity. Although it is relatively easy to prevent these unphysical transitions, preliminary calculations were not very promising.

The principal zeolite model that we will discuss is aluminum-substituted MFI. It is worthwhile to mention some of the unfruitful attempts to illustrate the fact that the enantioselective behavior requires very specific conditions. We first examined zeolites containing cages that can incorporate more than one molecule at a time. Seemingly, a difference in packing between identical and opposite enantiomers within a cage can be a driving force of enantiospecific adsorption. This hypothesis was tested for zeolite FAU, which contains cages of 1.2 nm. However, simulations at room temperature and lower (200 K) showed no significant difference between the enantiomeric ratio that was adsorbed and that of the external gas. Apparently, the alkane intermolecular interactions in this system are not sufficiently specific to differentiate between identical and opposite enantiomeric pairs. Still, this type of mechanism might well exist for stronger interacting chiral molecules such as polar or polarizable molecules. As expected, all-silica MFI (Silicate-1) also lacked chiral discrimination for temperatures of 298 K down to 100 K. MFI zeolites consist of a network of straight and zigzag channels that mutually intersect. The adsorption sites of 4-ethyl-4-methyloctane are located at the intersections of these channels, where the hydrocarbons can position each of the four branches in a separate exit-channel. Since the intersections can be occupied by only one single hydrocarbon while being relatively far separated, interaction between the adsorbed molecules is limited.

However, the picture changes when aluminum-substituted MFI is considered. The substitution of Si^{4+} with Al^{3+} results in a negatively charged site in the crystal framework, which is compensated by nonframework cations. The cation position can be influenced by nearby hydrocarbons, but also by an other distant cation, because of their long-range Coulombic interaction. In this way, the cations effectively mediate the hydrocarbon−hydrocarbon interactions at the different intersections.

We constructed 8 different aluminosilicates starting from the asymmetric unit of MFI, which has 12 crystallographically different silicon positions. Using the asymmetric unit

(8) Rouse, R. C.; Peacor, D. R. *Am. Mineral.* **1986**, *71*, 1494–1501.
(9) Harrison, W. T. A.; Gier, T. E.; Stucky, G. D.; Broach, R. W.; Bedard, R. A. *Chem. Mater.* **1996**, *8*, 145–151.
(10) Cheetham, A. K.; Fjellvaag, H.; Gier, T.; Kongshaug, K.; Lillerud, K.; Stucky, G. *Stud. Surf. Sci. Catal.* **2001**, *135*, 158.
(11) Tang, L.; Shi, L.; Bonneau, C.; Sun, J.; Yue, H.; Ojuva, A.; Lee, B.-L.; Kritikos, M.; Bell, R. G.; Bacsik, Z.; Mink, J.; Zou, X. *Nat. Mater.* **2008**, *7*, 381–385.
(12) Sun, J.; Bonneau, C.; Cantin, A.; Corma, A.; Diaz-Cabanas, M. J.; Moliner, M.; Zhang, D.; Li, M.; Zou, X. *Nature* **2009**, *458*, 1154–U90.
(13) Davis, M. E. *Top. Catal.* **2003**, *25*, 3–7.
(14) Jirapongphan, S. S.; Warzywoda, J.; Budil, D. E.; Sacco, A., Jr. *Chirality* **2007**, *19*, 508–513.
(15) Jirapongphan, S. S.; Warzywoda, J.; Budil, D. E.; Sacco, A., Jr. *Chirality* **2007**, *19*, 514–517.
(16) Clark, L. A.; Chempath, S.; Snurr, R. Q. *Langmuir* **2005**, *21*, 2267–2272.
(17) van Erp, T. S.; Caremans, T. P.; Dubbeldam, D.; Martin-Calvo, A.; Calero, S.; Martens, J. A. *Angew. Chem.−Int. Ed.* **2010**, *49*, 3010–3013.
(18) Dubbeldam, D.; Calero, S.; Vlugt, T. J. H.; Krishna, R.; Maesen, T. L. M.; Smit, B. *J. Phys. Chem. B* **2004**, *108*, 12301–12313.

and the space group, one can create the full unit cell and, hence, the whole (infinite) crystal. We focused on homogeneous distributions in which one of these Si atoms is systematically replaced by an Al atom, yielding a Si/Al ratio of 11:1. This ratio is close to the maximum concentration of Al atoms achieved in known MFI zeolite materials.[19] Four of these structures violate the Löwenstein rule, which forbids the presence of Al−O−Al linkages and were excluded. We name the remaining structures Al-1, Al-2, Al-3, Al-4, Al-5, Al-6, Al-8, and Al-11, after the index[20] of the substituted site. It is important to note that introducing Al atoms into the framework does not make the generated structures chiral. In this way, we obtained 8 different frameworks and 16 different adsorption systems, because we considered two types of cations: Na^+ and Ca^{2+}.

Force Fields. Alkane molecules were modeled using an united atom model in which each CH_x group is considered as a single interaction center to represent the CH_3, CH_2, and C groups. The bonded interactions include a harmonic bond, a bending potential, and a torsional angle potential. Dispersive interactions with the O atoms of the silica structure are assumed to dominate the silica−alkane interactions.[21] The silicon van der Waals interactions were taken into account through an effective potential with only the O atoms. Truncated and shifted Lennard-Jones (LJ) potentials[22] (at 12 Å) describe the interactions between the alkanes, as well as the interactions between the alkanes and the zeolite framework. The LJ parameters for alkane−zeolite interaction were optimized using inflection points on experimentally determined isotherms which provides a robust way to uniquely determine the strength (ε) and size (σ) parameters of the LJ potential.[18,23] The resulting force field reproduces the Henry coefficients, enthalpies, and entropies of adsorption, and maximum loading, extremely well.

The inclusion of aluminum in the zeolite framework and freely moving cations requires an extension of the parameter set. The charge distribution in the framework was considered static, i.e. fixed partial charges. Polarization effects were taken into account by adjusting the particle charges on the oxygen, depending whether they are connected to silicon or aluminum.[24] LJ parameters describing alkane−cation interactions were derived in refs 25 and 26, for Na^+ and Ca^{2+}, respectively. Only the LJ parameters between the central carbon and cations were yet not available in previous literature. We estimated these values based on Lorentz−Berthelot[27] mixing rules and extrapolation methods. However, the quality of these estimated values is of minor importance, as the chiral carbon is rather well-screened by the four alkyl chains. Table 1 summarizes the force-field parameters that were used in this work.

Table 1. Force-Field Parameters[a]

LJ Parameters						
	O	Na^+	Ca^{2+}	CH_3	CH_2	C
CH_3						
size, σ (Å)	3.48	2.65	2.6	3.76	3.86	5.07
strength, ε/k_B (K)	93	443.73	400	108	77.8	9.3
CH_2						
size, σ (Å)	3.58	2.95	2.8	3.86	3.96	5.17
strength, ε/k_B (K)	60.5	310	440.73	77.8	56	6.69
C						
size, σ (Å)	4.56	**3.65**	**3.6**	5.07	5.17	0.8
strength, ε/k_B (K)	10	**126**	**150.73**	9.3	6.69	6.38
Na^+						
size, σ (Å)	3.4			2.65	2.95	**3.65**
strength, ε/k_B (K)	23			443.73	310	**126**
Ca^{2+}						
size, σ (Å)	3.45			2.6	2.8	**3.6**
strength, ε/k_B (K)	18			400	440.73	**150.73**

Bond/Bend/Torsions/Charges

$$U_{bond} = {}^1/_2 k_1 (r - r_0)^2,\ k_1 = k_B \times 96500\ \text{K/Å}^2,\ \text{and}\ r_0 = 1.54\ \text{Å}$$

$$U_{bend} = {}^1/_2 k_2 (\cos\theta - \cos\theta_0)^2,\ k_2 = k_B \times 62500\ \text{K},\ \text{and}\ \theta_0 = 114$$

$$U_{torsion} = \sum_{i=0}^{5} \eta_i^{\alpha/\beta} \cos^i \varphi;\ \eta^{\alpha} = 1204.654, 1947.74, -357.845, -1944.666, 715.69, -1565.572;\ \eta^{\beta} = -357.845, 416.005, 0, 0, 0, -908.033\ \text{with}\ \alpha/\beta\ \text{torsion}$$

types: α = X−CH_2−CH_2−X, β = X−C−CH_2−X

partial charges O_{Si}, O_{Al}, Si, Al = −1.025, −1.2, 2.05, 1.75

[a] The LJ parameters for CH_3 and CH_4 were first given in ref 28 and extended for CH_2, CH, and C in ref 18. LJ parameters between alkanes and the zeolite framework was obtained using inflection points on isotherms.[18] Alkane−cation interactions were derived in refs 25 and 26. The internal bond parameters were taken from ref 29; bending and torsion parameters were taken from ref 30 and refs 18, 31, and 32, respectively. Partial charges were adopted from ref 24. Parameters not taken from previous literature were derived from extrapolation methods; these values are given in bold.

Simulation Details. The total simulation box consisted of 2 × 2 × 2 unit cells with a total size of 40.044 Å × 39.798 Å × 26.766 Å. We applied periodic boundaries. The zeolite was considered to be rigid. A flexible framework increases the computation time significantly, but it has hardly any influence on the adsorption of linear and branched alkanes.[33] The Coulombic interactions between the nonframework cations and the zeolite were calculated

(19) Jacobs, P. A.; Martens, J. A. *Stud. Surf. Sci. Catal.* **1987**, *33*, 47.
(20) Van Koningsveld, H.; Jansen, J. C.; Van Bekkum, H. *Zeolites* **1990**, *10*, 235–242.
(21) Kiselev, A. V.; Lopatkin, A. A.; Shulga, A. A. *Zeolites* **1985**, *5*, 261–267.
(22) Jones, J. E. *Proc. R. Soc. London, Ser. A* **1924**, *106*, 463–477.
(23) Dubbeldam, D.; Calero, S.; Vlugt, T. J. H.; Krishna, R.; Maesen, T. L. M.; Beerdsen, E.; Smit, B. *Phys. Rev. Lett.* **2004**, *93*, 088302.
(24) Jaramillo, E.; Auerbach, S. M. *J. Phys. Chem. B* **1999**, *103*, 9589–9594.
(25) Calero, S.; Dubbeldam, D.; Krishna, R.; Smit, B.; Vlugt, T. J. H.; Denayer, J. F. M.; Martens, J. A.; Maesen, T. L. M. *J. Am. Chem. Soc.* **2004**, *126*, 11377–11386.
(26) Garcia-Perez, E.; Dubbeldam, D.; Maesen, T. L. M.; Calero, S. *J. Phys. Chem. B* **2006**, *110*, 23968–23976.
(27) Allen,M. P.; Tildesley, D. J. *Computer Simulation of Liquids*; Oxford University Press: Boston, MA, 1989.
(28) Martin, M. G.; Thompson, A. P.; Nenoff, T. M. *J. Chem. Phys.* **2001**, *114*, 7174–7181.
(29) Nath, S. K.; Escobedo, F. A.; de Pablo, J. J. *J. Chem. Phys.* **1998**, *108*, 9905–9911.
(30) Martin, M. G.; Siepmann, J. I. *J. Phys. Chem. B* **1999**, *103*, 4508–4517.
(31) Ryckaert, J. P.; Bellemans, A. *Chem. Phys. Lett.* **1975**, *30*, 123–125.
(32) Ryckaert, J. P.; Bellemans, A. *Faraday Discuss.* **1978**, *66*, 95–106.
(33) Vlugt, T. J. H.; Schenk, M. *J. Phys. Chem. B* **2002**, *106*, 12757–12763.

using the Ewald summation;[34,35] this technique effectively accounts for the contributions of the mirror images in an infinite periodic lattice. The zeolite crystal consists of a total number of 2304 atoms (704 Si, 64 Al, 1536 O). The negative charge of the Al substituents is compensated by either 64 Na^+ or 32 Ca^{2+} cations, whose positions are highly influenced by the locations of the Al sites.

We exploited the fact that the potential energy field created by the rigid zeolite is static. For every type of nonframework atom (Na^+, Ca^{2+}, and CH_x), we precomputed and stored a potential energy grid, using a spacing of 0.1 Å. After this calculation, only the energies between the movable atoms must be computed explicitly since the interactions between the zeolite framework are directly interpolated from this grid. Numerical tests confirmed that differences between off-lattice and grid results are negligible. All simulations concerning enantioselective adsorption were done at a temperature of 298 K. Adsorption isotherms were calculated over a pressure range corresponding to fugacities of 10^{-12}, up to 10^2 Pa. Adsorption simulations of scalemic mixtures were performed at maximal loading, which implies a fugacity of >1 Pa.

Monte Carlo Modeling. Monte Carlo (MC) is the method of choice when sampling the equilibrium statistics of an adsorption process within the Grand Canonical ensemble. An important development that has made this type of simulations feasible is the configurational bias Monte Carlo (CBMC) approach.[30] The large molecules can only fit in the pores of the crystal when they have a very precise position and orientation. Therefore, random insertion moves will almost always result in configurations where some part of the molecules overlaps with the crystal framework, yielding a negligible acceptance rate. CBMC grows the molecule inside the framework in successive steps so that the energetically unfavorable overlaps are eliminated. Complementary to this, the molecules that have already been inserted can be translated and rotated over small distances and angles.

Starting from an empty framework, cations were inserted into the crystal until the right number was achieved for a correct charge balance, i.e., 32 Ca^{2+} or 64 Na^+. During this process, the cations were allowed to translate and be reinserted at random positions.

The adsorption isotherms were calculated for a pure-component system in which the external gas consists of R-enantiomers only. Starting from the low fugacities, hydrocarbons insertion and deletion attempts are followed by acceptance or rejection steps, to ensure detailed balance. In this way, for each value of the fugacity, we generate a distribution, according to

$$\rho[\mathbf{r}^N] \propto \frac{e^{-\beta[U(\mathbf{r}^N)-\mu N]}}{\Lambda^{3N}} = e^{-\beta[U(\mathbf{r}^N)]}(\beta f)^N \qquad (1)$$

which is the *unlabeled* Grand Canonical probability density.[36] Here, $\beta = 1/(k_B T)$ is the inverse temperature, where k_B is the Boltzmann constant and T is the temperature. Λ is the thermal wavelength and μ is the chemical potential of the alkanes, which is related to the fugacity (f) via the relation $\exp(\beta\mu) = \Lambda^3\beta f$. The parameter r^N is the multidimensional position vector that describes the positions of all N hydrocarbons in the zeolite. Note that we have simplified the notation, because ρ and U are dependent not only on the hydrocarbon positions, but also on their orientation and the positions of the cations.

After obtaining the adsorption isotherms, the enantiomeric specific adsorption characteristics were examined by studying the adsorption behavior of scalemic and racemic mixtures under maximal loading conditions. At high fugacity, whenever the maximum loading of 32 hydrocarbons was reached, addition and deletion moves attained zero acceptance and were, from that point onward, discarded to increase efficiency. Eliminating these moves effectively converts the system to the semi-Grand Canonical ensemble; the total number of adsorbed molecules remains constant, but individual numbers of R- or S-hydrocarbons can still vary. In this ensemble, the probability density can be derived from the fact that the two chemical potentials of the S- and R-alkanes (μ_S and μ_R, respectively) are directly related by the fugacity that is created by the S- or R-species only: $\exp(\beta\mu_{S/R}) = f_{S/R}\Lambda_{S/R}$. Because this $f_{S/R}$ term refers to the conditions in the external reservoir and each molecule is assumed to have an equal impact on the fugacity, we can simply write $f_{S/R} = \xi_{S/R} f$, where $\xi_S = 1 - \xi_R$ denotes the fractional content of S-enantiomers in the gas-phase and ξ_R represents that of the R-enantiomers. The total number of S- and R-enantiomers is always constant and equal to $N = N_S + N_R$. This finally leads to the following probability density:

$$\begin{aligned} \rho[\mathbf{r}_S^{N_S}, \mathbf{r}_R^{N_R}] &\propto \frac{e^{-\beta[U(\mathbf{r}_S^{N_S}, \mathbf{r}_R^{N_R}) - \mu_S N_S - \mu_R N_R]}}{\Lambda_S^{3N_S}\Lambda_R^{3N_R}} \\ &= e^{-\beta[U(\mathbf{r}_S^{N_S}, \mathbf{r}_R^{N_R})]}\beta^N f_S^{N_S} f_R^{N_R} \\ &= e^{-\beta[U(\mathbf{r}_S^{N_S}, \mathbf{r}_R^{N_R})]}(\beta f)^N \xi_S^{N_S}\xi_R^{N_R} \\ &\propto e^{-\beta[U(\mathbf{r}_S^{N_S}, \mathbf{r}_R^{N_R})]}\xi_S^{N_S}\xi_R^{N_R} \end{aligned} \qquad (2)$$

Note that N_S and N_R denote the number of S- and R-molecules, respectively, in the adsorbed phase, while ξ_S and ξ_R respectively denote the fractional content of the same species in the gas phase. Because of the presence of the intermolecular potential U, the average fraction of adsorbed S-molecules does not have to reflect that of the gas phase or $\overline{N_S}/N \neq \xi_S$. Clearly, once the fugacity is above the maximal loading limit, it no longer affects the equilibrium statistics. The equilibrium distribution is dependent only on temperature T and the enantiomeric ratio ξ_S in the gas phase.

For each Al-substituted MFI zeolite and each type of cation, we performed nine different statistical ensembles (defined by $\xi_S = 0.1, 0.2, ..., 0.9$) while the temperature is always set at 298 K. MC moves comprise translations, rotations, and regrowth. The latter is basically a consecutive deletion and CBMC insertion move at the same position. The chirality of the new molecule can be different from the deleted one. However, under these conditions, at maximal loading, even the use of CBMC becomes problematic and

(34) Ewald, P. *Ann. Phys.* **1921**, *369*, 253–287.
(35) Frenkel, D.; Smit, B. *Understanding Molecular Simulation*, 2nd ed.; Academic Press: San Diego, CA, 2002.
(36) Norman, G. E.; Filinov, V. S. *High Temp.* **1969**, *7*, 216–222.

acceptance probabilities of 0.02% are typical. Although the above acceptance and number of required simulation ensembles are still doable, given present computer resources, the situation is complicated further by an extremely slow ergodicity, because of the presence of metastable states. The present MC scheme cannot easily connect all different acceptable configurations, because of the existence of complex clusters where molecules of the same type or, on the contrary, of the opposite type have specific arrangements. The CBMC move that changes the identity of one molecule will always break up the energetically favorable situation and is therefore rejected, because it is unable to flip a whole pair or cluster of molecules. To improve our statistics, we developed two novel MC moves.[37] First, we invoked a replica exchange procedure, where the configuration of a simulation with a particular gas ratio ξ_S is swapped for the configuration of a neighboring gas ratio (± 0.1). Therefore, ξ_S has the same role as temperature in the standard parallel tempering algorithm. Detailed balance rules can be derived in a similar fashion.[37] Second, we applied a chiral inversion move in which all atomic positions are mirrored in a symmetry plane of the fixed zeolite framework, changing all enantiomers to their opposite type. Only after the introduction of these two moves, we obtained well-converged and reproducible results that are insensitive to the starting conditions.

Simulations are performed in cycles. Each cycle consists of inner MC steps.[38] In each MC step, first a random system is chosen. The number of inner steps is $N + N_{sm}$, where N is the number of molecules of the current system and N_{sm} is the number of system moves. This definition of cycles instead of MC steps is mainly because it allows a definition that is relatively independent of the system size. Next, for each MC step, a random number is drawn, deciding to do a system move or a move on the molecules. There are two system moves: chiral inversion and the replica exchange, while the molecule moves are translation, rotation, and regrow in place. The relative fraction of molecule moves is chosen such that, on average, each cycle consists of ~150 translations, ~50 rotations, and ~100 CBMC moves for all molecules in total. The CBMC move has an equal probability to grow either the same or the opposite enantiomeric form of the molecule that is replaced. In addition, each cycle performs, on average, two replica-exchange moves, where the system with enantiomeric fraction ξ_S is switched with either $\xi_S + 0.1$ or with $\xi_S - 0.1$, and one chiral-inversion move.

For each system, 50 000 initialization cycles were run, starting from an empty crystal. After initialization, all zeolite systems were loaded at maximum. Two up to eight independent simulations of 40000 cycles were performed for each Al-framework, cation type, and ξ_S value. A larger amount of CPU time was spent for those systems that showed significant deviations from the trivial line during the first preliminary runs. The statistical error bars were calculated from the standard deviation of the independent simulations. A more-detailed description of the simulation methods can be found in refs 18 and 37.

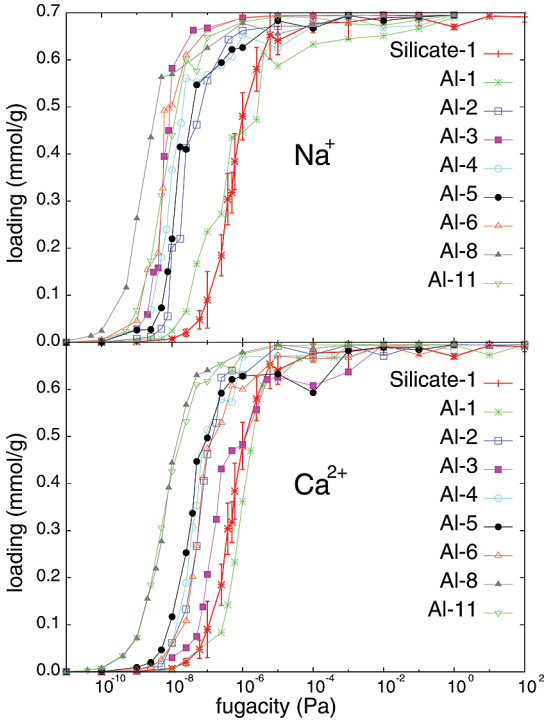

Figure 2. Adsorption isotherms for all eight aluminum-substituted MFI zeolites with either Na^+ (top) or Ca^{2+} (bottom) and all-silica MFI (Silicalite-1) without cations. Error bars are only given for the Silicate-1 curve; error bars on the other curves are similar in size.

Results

Adsorption Isotherms of Pure-Component Systems. We calculated adsorption isotherms at 298 K in the Grand Canonical ensemble for an enantiopure gas using CBMC for all 16 aluminum-substituted MFI(Na^+,Ca^{2+}) systems and Silicate-1 (see Figure 2). The location of the Al atoms clearly influences the shape of the isotherms. This result is contrary to that which has been found for linear alkanes in MFI.[39,40] This has interesting consequences, because the location of the Al atoms is difficult to access experimentally.[41,42] Computational modeling of adsorption isotherms of linear alkanes has been exploited to characterize Al distributions in several zeolites.[39] The location of the aluminum in the framework affects the position of the ions, which, in turn, influences the adsorption behavior of the alkanes. However, a certain class of zeolites (including MFI) was insensitive to the aluminum distribution. In the case of MFI, this is probably due to the fact that, at low pressures, small alkanes preferentially adsorb in the channels, whereas the cations are likely to be situated in the channel intersections.[40] However, branched alkanes tend to reside in the intersections, which

(37) van Erp, T. S.; Dubbeldam, D.; Caremans, T. P.; Calero, S.; Martens, J. A. J. Phys. Chem. Lett. **2010**, *1* (14), 2154−2158.
(38) Dubbeldam, D.; Calero, S.; Ellis, D. E.; Snurr, R. Q. RASPA 1.0: Molecular Software Package for Adsorption and Diffusion in (Flexible) Nanoporous Materials, 2009.
(39) Garcia-Perez, E.; Dubbeldam, D.; Liu, B.; Smit, B.; Calero, S. *Angew. Chem.−Int. Ed.* **2007**, *46*, 276–278.
(40) Liu, B.; Garcia-Perez, E.; Dubbeldam, D.; Smit, B.; Calero, S. *J. Phys. Chem. C* **2007**, *111*, 10419–10426.
(41) Van Bokhoven, J. A.; Lee, T.-L.; Drakopoulos, M.; Lamberti, C.; Thiss, S.; Zegenhagen, J. *Nat. Mater.* **2008**, *7*, 551–555.
(42) Sklenak, S.; Dedecek, J.; Li, C.; Wichterlova, B.; Gabova, V.; Sierka, M.; Sauer, J. *Phys. Chem. Chem. Phys.* **2009**, *11*, 1237–1247.

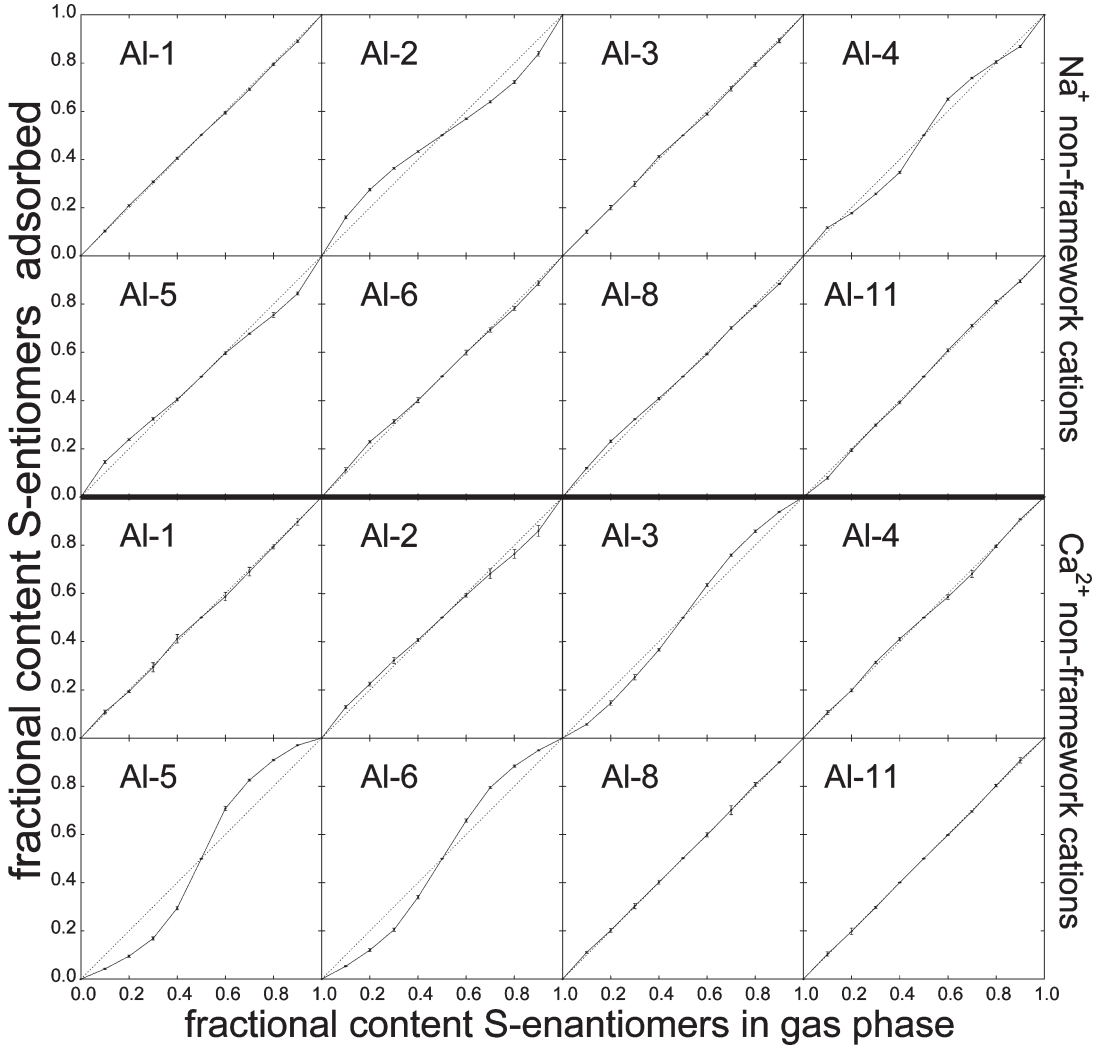

Figure 3. Adsorbed fractional content of the S-enantiomer against the same fraction in the external gas phase for all 16 MFI systems. Most of the curves, like Al-1(Na^+), are simply straight, which indicates that the enantiomeric ratio in the adsorbed phase is identical to that in the gas phase. All curves are symmetric and pass through the (0.5,0.5) point, which is a direct result of the zeolites being not chiral by themselves. However, if one enantiomeric form is more available in the reservoir, its relative fraction that adsorbs might either be higher (like Al-5(Ca^{2+})), lower (like Al-2(Na^+)), or either way, depending on the relative concentration (Al-4(Na^+)).

explains the considerable changes in isotherms, compared to Silicate-1. It also suggests that the computational approach for localizing the Al positions might actually work if branched alkanes are used instead of linear ones.

Above 1 Pa, all aluminosilicate systems are in the saturation regime. The total number of hydrocarbons is constant and is equal to 6.95 mmol/g, which corresponds to four molecules per unit cell. The calculated isotherms, especially with Ca^{2+}, can be categorized in three groups. One group at the left, which are the Al-8 and Al-11 substitutions, increase rapidly at very low pressures. Also, there is one isotherm (Al-1 and, to some extent, Al-3) that, more or less, follows the Silicate-1 curve. All other others lie between these results. The possibility of enantioselective adsorption is mediated by the influence of cations. Therefore, it is to be expected that, if this effect exists, it will be reflected by a significant deviation in the isotherm, compared that of Silicate-1. On the other hand, it is tempting to conclude that the isotherms that deviate most (Al-11, Al-8) are also those that show the strongest enantiospecific adsorption; however, this is not the case. We will revisit this point in section 4.

Enantiospecific Adsorption of Scalemic and Racemic Mixtures. Under maximal loading conditions, we examined the adsorption behavior of scalemic and racemic mixtures for all 16 systems. Figure 3 shows the fraction of adsorbed S-molecules against the same enantiomeric ratio in the gas phase for all 16 cases. A majority of the examined systems simply show a straight line. This implies that the fractional content of S- and R-enantiomers adsorbed in the zeolite is identical to that of the external gas. For the Ca^{2+}-containing systems, this is the case for Al-1, Al-4, Al-8, and Al-11. On the other hand, Al-3(Ca^{2+}), Al-6(Ca^{2+}), and especially Al-5(Ca^{2+}) do deviate significantly from the diagonal. For the Al-distributions with Na^+ serving as the nonframework cation, almost all combinations give straight lines, with the notable exception of Al-2 and Al-4.

Note that all curves are symmetric and pass through the (0.5,0.5) point. In other words, if the gas contains a racemic mixture, the resulting adsorbed phase will be racemic as well. This is a natural result of the symmetry in the system, because none of the Al-substituted zeolites are chiral. For scalemic mixtures, the enantiomeric ratio

in the adsorbed phase can differ from that in the gas phase in two ways. The curves can either display an S-form, like Al-5(Ca^{2+}), or its inverse, like Al-2(Na^{+}). The first case indicates an homoselective adsorption process. The enantiomeric form that is already dominantly present in the gas phase is even more enriched in the adsorbed phase. This is due to a favorable interaction between enantiomers of the same type. The second case is heteroselective adsorption, which indicates a favorable interaction between adsorbed molecules of opposite types. Al-4(Na^{+}) is special, because it crosses the diagonal three times.

Number Distributions. The results of Figure 3 can be further analyzed by computing the number distributions $P(N_S)$, which is the probability to have exactly N_S S-enantiomers in the system. Theoretically, these distributions are obtained via eq 2 by

$$P(N_S) \equiv \frac{\frac{1}{N_S!(N-N_S)!}\int d\mathbf{r}_S^{N_S}\, d\mathbf{r}_R^{N-N_S}\rho[\mathbf{r}_S^{N_S},\mathbf{r}_R^{N-N_S}]}{\sum_{N_S'=0}^{N}\frac{1}{N_S'!(N-N_S')!}\int d\mathbf{r}_S^{N_S'}\, d\mathbf{r}_R^{N-N_S'}\rho[\mathbf{r}_S^{N_S'},\mathbf{r}_R^{N-N_S'}]} \tag{3}$$

Note again that we used a simplified notation. Besides integration over the hydrocarbon positions, we should also integrate out all possible molecular orientations and cation positions. The divisors $N_S'!(N-N_S')!$ prevent overcounting. Note that the probability distributions in eqs 1 and 2 are definitions of an unlabeled macrostate.[36] This implies that interchanging two molecules of the same type results in the same state and should not be counted twice. In practice, $P(N_S)$ is simply calculated by examination of the MC run at discrete intervals and to keep track how often N_S takes a certain value. An insightful comparison can be made with the theoretical result of an enantio-unspecific system. Suppose that $U(\mathbf{r}_S^{N_S},\mathbf{r}_R^{N_R})$ is independent to the chiral identity of the molecules then $\int d\mathbf{r}_S^{N_S'}\, d\mathbf{r}_R^{N-N_S'}\exp(-\beta U)$ is a constant and equal for all N_S'. So, we can rewrite eq 3 using eq 2 as follows:

$$\begin{aligned} P(N_S) &= \frac{\frac{N!}{N_S!(N-N_S)!}\xi_S^{N_S}\xi_R^{N-N_S}}{\sum_{N_S'=0}^{N}\frac{N!}{N_S'!(N-N_S')!}\xi_S^{N_S'}\xi_R^{N-N_S'}} \\ &= \frac{\binom{N}{N_S}\xi_S^{N_S}\xi_R^{N-N_S}}{\sum_{N_S'=0}^{N}\binom{N}{N_S'}\xi_S^{N_S'}\xi_R^{N-N_S'}} \\ &= \binom{N}{N_S}\xi_S^{N_S}(1-\xi_S)^{N-N_S} \end{aligned} \tag{4}$$

with the binomial coefficients being defined as

$$\binom{n}{m} \equiv \frac{n!}{m!(n-m)!}$$

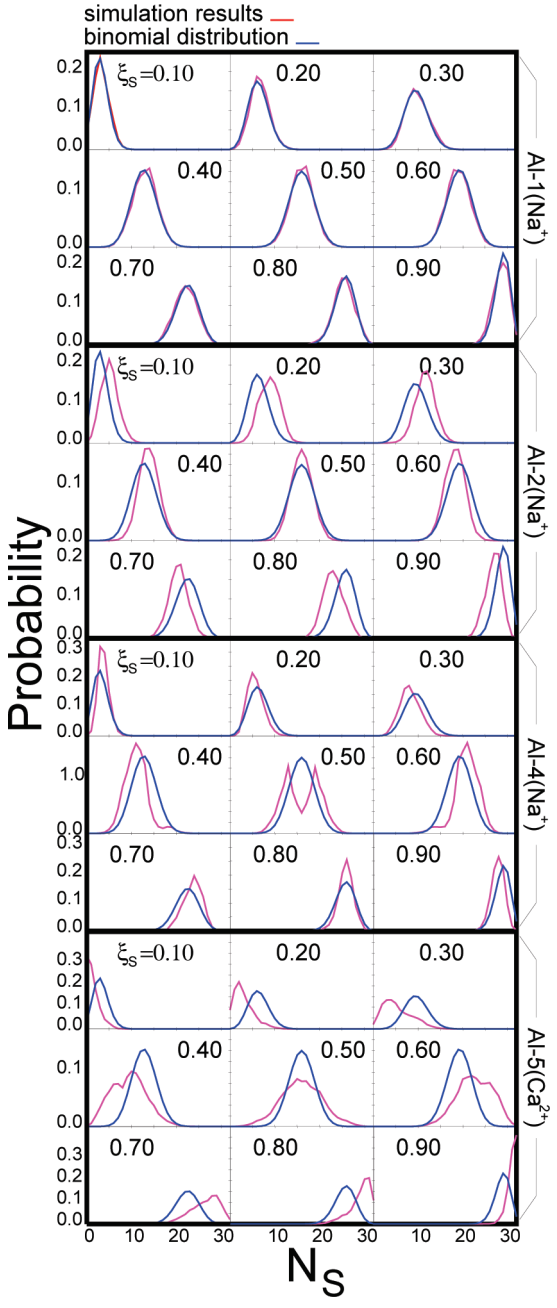

Figure 4. Number distributions (red) for cases Al-1(Na^{+}), Al-2(Na^{+}), Al-4(Na^{+}), and Al-5(Ca^{2+}), together with the binomial distribution (blue) for the nine values of ξ_S.

In the last line, we have made use of the binomial theorem:

$$\sum_{k=0}^{n}\binom{n}{i}y^k x^{n-k} = (x+y)^n$$

and $\xi_S + \xi_R = 1$. The final distribution (eq 4) is the well-known binomial distribution.

In Figure 4, we show the calculated distributions for cases Al-1(Na^{+}), Al-2(Na^{+}), Al-4(Na^{+}), and Al-5(Ca^{2+}), together with the binomial distribution for the nine values of ξ_S. Clearly, the Al-1(Na^{+}) system, which does not show any enantiospecific adsorption, has distribution curves that lie on top of the binomial ones. The distribution of Al-2(Na^{+}) at $\xi_S = 0.5$ is narrower and higher than the

binomial curve. This is indicative of its heteroselective adsorption. In contrast, the homoselective Al-5(Ca^{2+}) system shows a distribution that is much lower and broader than the binomial one. The strongest difference is found for Al-4(Na^{+}). This distribution is double-peaked for $\xi_S = 0.5$ with a local minimum at $N_S = 16$. Apparently, this system wants to be loaded with either S- or R-molecules, but not both at the same time. A macroscopic Al-4(Na^{+}) system will consequently have large regions with only S- or only R-alkanes assembled together. Still, if the means of the distributions are considered, Al-4(Na^{+}) is much less deviating than, for instance, Al-5(Ca^{2+}).

Discussion

Alkane and Cation Positioning and Orientation in Aluminum Frameworks. To understand the mechanism of the enantioselective effect in MFI zeolites and their relationship with the different aluminum frameworks, we will have a closer look at the molecular configurations for Al-5(Ca^{2+}) and Al-11(Ca^{2+}). The first shows the strongest enantioselectivity, while the other is not selective. Figure 5a shows a typical representation of the internal configuration of the hydrocarbons in Al-5(Ca^{2+}) for $\xi_S = 0.7$. The degree of order is striking. All S-molecules show an almost-identical orientation. Butyl and methyl groups are aligned along the zigzag channel, with all butyl chains pointing to the same direction. The ethyl and propyl group are positioned along the straight channels, with the latter always pointing away from the cation. Naturally, this specific orientation gives restrictions to all four branches of the hydrocarbon. This implies that R-alkanes cannot fit in the same pattern and, therefore, create unavoidable mismatches. The free-energy benefit of having as much order as possible pushes out the R-enantiomers in favor of the S-alkanes. In this figure, 30 out of 32 molecules are left-handed, while 22 would be expected, based on its gas-phase ratio. Also, the cations follow a clear motif and alternate between two antipodal adsorption sites, which resembles a sequence of knight moves on a chessboard. In contrast, the orientation of the remaining R-enantiomers is rather unpredictable. It resembles the molecular orientation of both S- and R-molecules in Silicalite-1.[17] Apparently, if the pattern must be broken, it does not matter how this is done.

Figure 5b shows a magnified view of a single hydrocarbon with a cation at one of the intersections. The Ca^{2+} ion, which counterbalances the negative charge, is positioned between the aluminum pair in one of the 10-rings that forms the access to a zigzag channel. Because the distance between the Al atoms is relatively large, it is energetically more favorable to stay closer to one of them than to be in the exact middle. The cation is closely accompanied (< 4 Å) by the methyl, the central carbon, and the first carbons of the ethyl and butyl group. This apparently comprises the optimal alkane-cation packing at the intersection. The asymmetric location of the cation and its close connectivity with the carbons turns out to be crucial for its enantioselective adsorption behavior.

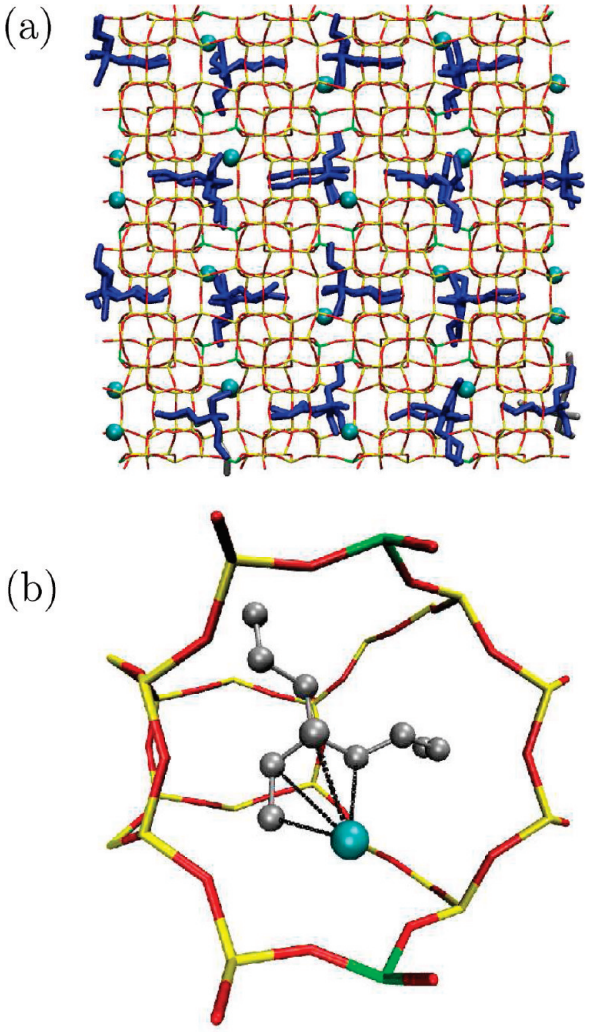

Figure 5. (a) Snapshot of 4-ethyl-4-methyloctane molecules (S/R gas ratio = 7:3) in Al-5(Ca^{2+}). Zigzag and straight channels are oriented, respectively, horizontally and vertically in the plane of the page. S- and R-enantiomers are colored blue and gray, respectively. The blue spheres represent the Ca^{2+} cations. (b) Magnification of the hydrocarbon-cation packing at one specific intersection; the zeolite framework colors denote oxygen (red), silicon (red), and aluminum (green), and the dashed lines between the cation and the carbons are drawn for distances of < 4 Å.

A similar figure for the Al-11(Ca^{2+}) system is shown in Figure 6. Compared to Figure 5, there is much less structure. There is no detectable preferred orientation nor clear correlations between neighboring molecules, similar to that found for Silicalite-1.[17] Al-11 has its two alumina in one of the 6-rings, which are opposing the entrances of the zigzag channels (see Figure 6b). Again, the cation is surrounded by the central carbon and the first beads of three molecular branches. However, the branch that is pointing away seems to be chosen more arbitrary than in Al-5(Ca^{2+}), where it is always the propyl group. The cation that is between the two Al atoms is not blocking the zigzag channels. Moreover, because the Al atoms are closer than in Al-5, the cation takes an equidistant position between the two Al atoms. Indeed, if we re-examine the full configuration of Figure 6a, we notice that all cations lie on the same horizontal lines that separates the intersection in two equal halves. The symmetric positioning is unable to create a preference for one of the two enantiomers.

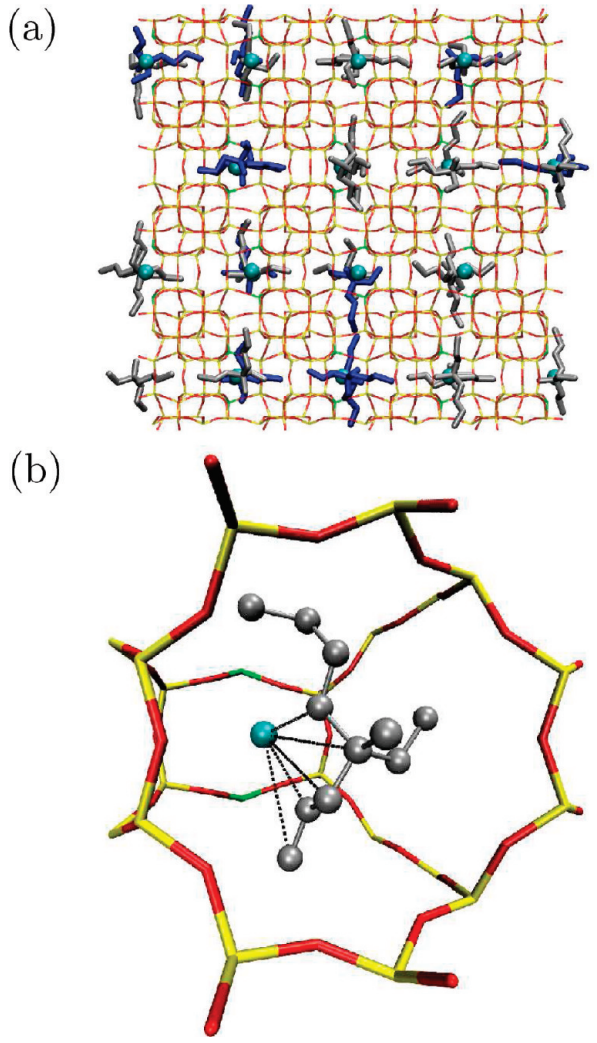

Figure 6. (a) Adsorption configuration of hydrocarbons (S/R gas ratio = 3:7) in Al-11(Ca^{2+}); the color scheme is the same as that in Figure 5. (b) Enlargement of the hydrocarbon-cation packing at an intersection.

Chiral Cell Model. Here, we explain the occurrence of homoselective or heteroselective adsorption, making use of the concept of *chiral cells*.[17] As discussed above, the cation will always lie between two Al atoms, to counterbalance the negative charge. However, when the Al atoms are sufficiently far away from each other, like in the Al-5(Ca^{2+}) case, the energetically optimal position for the cations is not exactly in the middle. A lower energy is obtained for an asymmetric position, where the cation is closer to one of the two. This results in two possible adsorption sites and the occurrence of a chiral cell, because of a local breaking of symmetry (see Figure 7).

The asymmetric positioning of the cations, together with the presence of two different types of channels, makes each exit at the intersection physically different from each other, creating an effective chiral environment. This causes a mutual interaction; the positioning of the cation will favor one specific enantiomeric form. Vice versa, if either an S- or R-molecule is adsorbed in the cell, it will try to position the cation close to the Al atom, which suits it best. The cations, which are influenced by their electrostatic repulsion, try to maximize their separation. This induces nonlocal correlations between

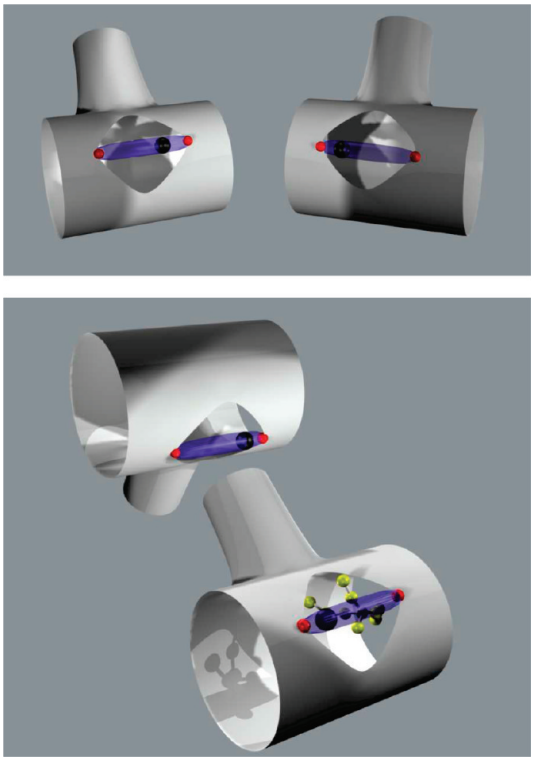

Figure 7. Illustration of "chiral cells". Straight and zigzag channels are represented by the big and small cylinders, respectively. Aluminum sites are colored red. The purple region indicates the constraint mobility of the Ca^{2+} cation (black sphere). The Ca^{2+} can move between the two closest Al atoms. However, it will obtain its lowest energy when it is not in the middle, but relatively close to one Al atom. The asymmetric positioning of the cation makes each exit channel distinctively different from each other, creating a "chiral cell". The top panel shows the two possible chiral cells that are its mirror images. The cell on the left preferentially adsorbs the R-enantiomers, while the cell on the right prefers the S-type. The bottom panel shows that a cell of a given chirality influences the type of chirality that is created in a neighboring cell. The adsorption of an S-enantiomer will place the cation in its preferential Al site. In the neighboring intersection, the cation takes the position that lies farthest away from the other cation. Therefore, the induced chirality here is of the same type as in the other cell and will, most likely, also be occupied by an S-enantiomer.

the cells (see Figure 7). Hypothetically, the adsorption of the first enantiomer would determine a chiral environment throughout the whole crystal, so that only molecules of the same type can enter. Under realistic thermodynamic conditions, the last statement should be viewed as an oversimplification; it does, however, correctly describe the main principle why Al-5(Ca^{2+}) tends to favor that enantiomeric form that is already dominant in the reservoir. We also examined the positions of the Ca^{2+} cations in the absence of the hydrocarbons. Remarkably, even in an empty framework, the cations already seem to take very specific positions, dictated by the positions of the neighboring cations. The hydrocarbons seem to cause only little disturbance to the cation position; however, their presence is crucial for determining which adsorption site is chosen most frequently.

On the other hand, the Al-5(Na^{+}) is much less enantiospecific. It even shows an opposite trend toward heteroselective adsorption. Although the Al-distribution is the same, there are twice as many cations present. One Na^{+} is placed between the alumina in the intersection, the other is situated in the straight channel (see Figure 8). The adsorption sites of

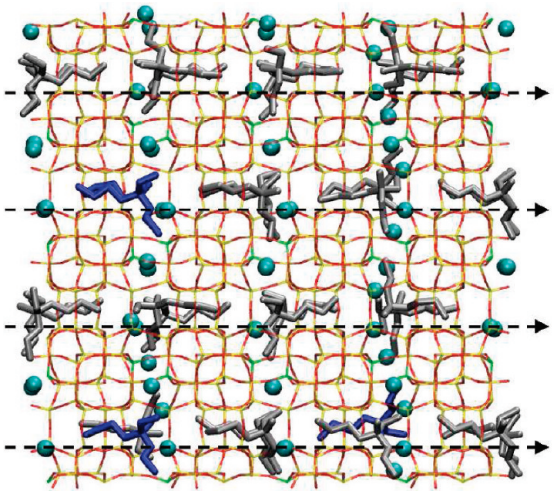

Figure 8. Adsorption configuration for the Al-5(Na^+) system with $\xi_S = 0.1$; the color scheme is the same as that given in Figure 5. Half of the Na^+ ions lie inside the intersections; the others lie more outside of it, inside the straight channels. Dashed arrows indicate the horizontal alignment of the Na^+ cations in the intersections. This is similar to the Ca^{2+} ions in Al-11 but is contrary to Ca^{2+} in Al-5 (see Figures 5 and 6). However, different to Al-11(Ca^{2+}), the Na^+ cation positioning is not symmetric. Each intersection turns into a chiral cell but adjacent cells are of opposite chirality; the change in curvature of the zigzag channels is not compensated by a "cation jump" as in Al-5(Ca^{2+}).

Na^+ in the intersection are almost identical to that of Ca^{2+}. However, if we examine these cations from left to right, we see that Na^+ is not alternating as Ca^{2+} does in the same framework. The presence of the additional charges of the other cations in the straight channel prevents this alternating pattern. As a result, the Na^+ in the intersections are horizontally aligned just as Ca^{2+} is in Al-11 (see Figure 6). However, in contrast to Al-11, this alignment is not exactly in the middle of the intersection. Hence, each intersection forms a chiral cell as in Al-5(Ca^{2+}), but neighboring cells preferentially show chirality of the opposite type. Both types of chiral cells are equally present, which explains the tendency toward a more racemic adsorbed phase.

Quantifying the Enantiomeric Effect. The purity of an adsorbed mixture of R- and S- enantiomers is commonly expressed with the aid of the enantiomeric excess (*ee*). For a racemic mixture, it is defined as

$$ee = \frac{\xi_S^a - \xi_R^a}{\xi_S^a + \xi_R^a} \tag{5}$$

where $\xi_{S/R}^a$ is the S/R-enantiomeric fraction in the adsorbed phase. However, as explained above, for reasons of symmetry, a racemic gas will also result in $\xi_S^a = 0.5$, so that enantiomeric excess will always be zero ($ee = 0$). Therefore, eq 5 is not very convenient to describe the type of enantioselectivity discussed here. Therefore, we give an alternative expression that we will call *ee**, which we define as

$$ee^* \equiv \mathrm{Extr}[\xi_S^a(\xi_S) - \xi_S]_{\{0<\xi_S<0.5\}} \tag{6}$$

where Extr denotes the extremum on the interval [0:0.5]. This is equal to the maximal vertical displacements, either positive or negative, from the diagonal in Figure 3. Heteroselective adsorption will result in a positive value for *ee**, while it is negative for homoselective adsorption.

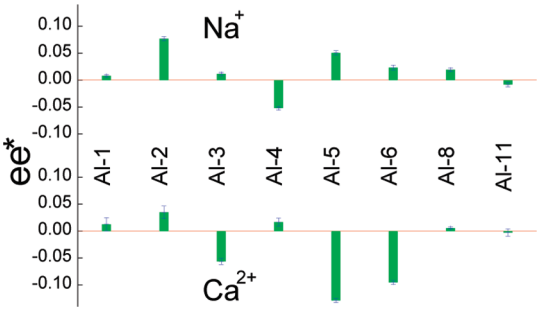

Figure 9. Enantiomeric excess values *ee**, as defined by eq 7, for all 16 Al-substituted MFI systems. The zeolites with Na^+ are mainly positive, which is a sign for heteroselective adsorption. *ee** values for Ca^{2+} are mainly negative (homoselective).

In practice, we use the fact that all curves in Figure 3 are symmetric, so that $\xi_S^a(\xi_S) - \xi_S = (1 - \xi_S) - \xi_S^a(1 - \xi_S)$. Therefore, we can obtain a numerically more-accurate value by taking its average:

$$ee^* = \frac{1}{2}\mathrm{Extr}[\xi_S^a(\xi_S) - \xi_S^a(1 - \xi_S) - 2\xi_S + 1]_{\{\xi_S = 0.1, \ldots, 0.4\}} \tag{7}$$

which was used for our numerical calculations. Figure 9 shows the *ee** values for all 16 systems. In most cases, the *ee** does not exceed 5%. For the cases where it does exceed 5%, the systems with Ca^{2+} cations (Al-3, Al-5, and Al-6) only display homoselective adsorption, whereas the Na^+ systems (Al-2 and Al-5) produce heteroselective adsorption. This results from a different distribution of charges, as explained in the previous section. The behavior of the Al-4(Na^+) is more complicated, because of the particular position of alumina in the framework.

Figure 10 shows a simplified representation of the MFI framework. An intersection of the framework is characterized by two neighboring 10-rings, giving access to the zigzag channels. The 10-rings are also connected to each other by two 6-rings. For Al-8 and Al-11, the Al atoms are situated in the 6-rings (red color, upper intersection). Note that these systems also show the fastest increasing adsorption isotherms (see Figure 2). The surrounding of cations by several C atoms in the Al-substituted zeolites (see Figures 6b and 5b) supports the adsorption at much lower pressures than those in Silicalite-1. The 6-ring frameworks show an even better adsorption, compared to the others, because it is not blocking the zigzag channel which allows more freedom for the molecules to enter. The Al-1 framework shows an aluminum pair that is situated in the 10-ring, but too much at the outside to have an effect. The corresponding isotherm closely resembles the Silicalite-1 curve, indicating a weak cation hydrocarbon interaction. Both extremes do not show a significant enantiomeric effect, as can be concluded from Figure 9. Surprisingly, the aluminum frameworks that belong to the intermediate group of isotherms in Figure 2 show the highest *ee** values. This group of frameworks does impose restrictions to the hydrocarbon orientation, because it has its Al-pair near the center of the 10-ring. In addition, the relatively large distance between the alumina results in an asymmetric positioning of the cation, which creates an effective local chirality (chiral cell) of the adsorbent. Aluminum

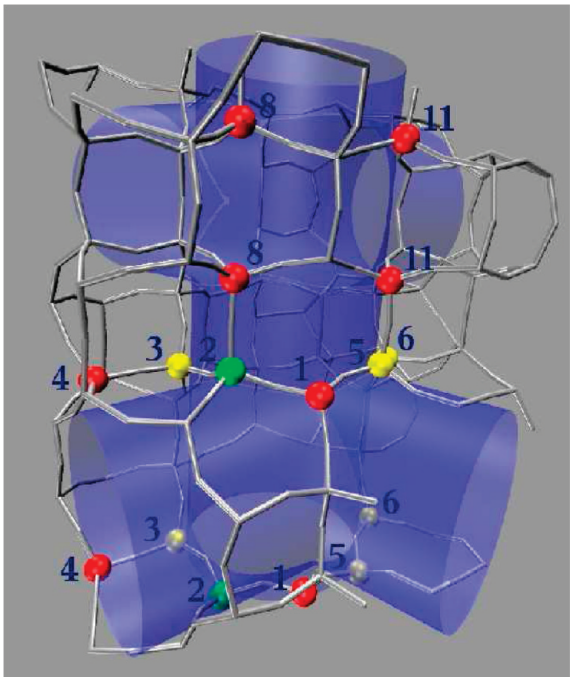

Figure 10. Possible Al-substitution sites. The numbers indicate their crystallographic index.[20] Only those sites are shown that do not violate Löwenstein's rule. Considering the cations with the highest enantioselectivity, the positions with a green color show heteroselective adsorption. The yellow positions yield homoselective adsorption. The red color does not show any enantioselectivity ($ee^* < 5\%$) for any type of cations.

pairs that are more outward from the center show an enantioselectivity that is less pronounced.

Conclusions

Using molecular simulations, we have investigated the enantioselective adsorption characteristics of 4-ethyl-4-methyloctane in achiral aluminum-substituted MFI zeolites with Na^+ or Ca^{2+} cations. Although all aluminosilicates are achiral, some of them exhibit considerable chiral discrimination power, as long as the adsorbing gas consists of a scalemic mixture. If one of the enantiomers is already present in a higher concentration than its opposite form, this concentration might either increase or decrease upon adsorption. These two types of enantiospecific adsorption—homoselective and heteroselective, respectively—are enforced by a particular positioning of the cations in the channel's intersections. The inclusion of Ca^{2+} causes the first type of adsorption, whereas Na^+ mainly results in heteroselective adsorption. Introducing the concept of *chiral cells*, we can explain both types of adsorption or the lack of it. The key ingredient for enantioselectivity is that the Al-framework provides an aluminum pair inside the intersection along the center of the 10-ring, which forms the entrance of the zigzag channel. The cation that resides between the alumina is then taking an asymmetric position, where it imposes stronger restrictions to one of the enantiomers. Each intersection becomes an effective chiral cell, which is correlated with its neighbors, because of the long-range repulsion between the ions. The distribution of charges in the Ca^{2+} systems has a tendency to create chiral cells of the same type, whereas the double number of Na^+ ions favors neighboring cells to be of opposite chirality.

Our findings are not restricted to MFI or chiral hydrocarbons. The enantioselective adsorption mechanism in achiral zeolites is a fundamentally new mechanism that might be exploited for technical applications in the future. A relatively straightforward application would be the purification of an enantio-enriched feed (for instance, that obtained from a chiral catalytic process). Generally, it would not be profitable to enrich racemic input feed by adding some enantiopure compound. In a sequential batch process the same quality of enantiopure product can be reobtained but normally in lower quantity. However, a simple mathematical model[43] suggests that there exists a critical break-even point, beyond which a hypothetical pressure-swing-adsorption process can create a final amount of enantiopure product that is larger than is needed to enrich its own racemic input feed. As the selectivity becomes stronger at low temperatures, all enantioselective adsorption systems can be brought into this regime. However, the critical temperature is rather low for the present system.[43] Based on some simple geometrical rules, our theoretical model is able to predict the possibility of having enantioselective adsorption in other zeolite materials. The efficiency of such an application would considerably depend on the aluminum distribution, but a strict ordering is not essential.[17] Hitherto, only little attention has been given to the development of selective synthesis methods that can control the positioning of the Al sites. The location of the Al positions is not even known for almost all synthesized metal-substituted zeolites. However, a very rapid evolution is taking place in this field.[41,42] Also, here, the presented simulations might be instrumental, because they provide a way to determine this Al location, because isotherms (like Figures 2 and 3) seem to provide fingerprints of specific Al frameworks. Once a technique for the exact determination of Al siting is developed, control and design might quickly follow. The design of the right template molecule for the zeolite synthesis is probably key in achieving this, because it is known to be not only structure-directing but is also largely responsible for the Al positioning.[44] The impact of our findings for future applications is still difficult to foresee, but it certainly deserves further investigation.

Acknowledgment. We acknowledge the Flemish Government for long-term structural support via the Center of Excellence (CECAT), the Concerted Research Action (GOA), and Methusalem Funding. T.P.C. acknowledges the Flemish IWT for a Ph.D. grant. T.S.v.E. and J.A.M. participated in Interuniversity Attraction Pole (IAP). S.C. acknowledges the funding via the CTQ2007-63229 and P07-FQM-02595 projects.

(43) van Erp, T. S.; Dubbeldam, D.; Calero, S.; Martens, J. A. in progress **2009**.
(44) Sastre, G.; Fornes, V.; Corma, A. *J. Phys. Chem. B* **2002**, *106*, 701–708.